

Analysis of Proline Substitutions Reveals the Plasticity and Sequence Sensitivity of Human IAPP Amyloidogenicity and Toxicity

Zachary Ridgway, Charles Frederick, Samuel Eldrid, Alexander Zhyvoloup, Aisha Ben-Younis, Daeun Noh, Konstantinos Thalassinos, and Daniel P. Raleigh

Biochemistry, **Just Accepted Manuscript** • DOI: 10.1021/acs.biochem.9b01109 • Publication Date (Web): 10 Jan 2020

Downloaded from pubs.acs.org on January 15, 2020

Just Accepted

“Just Accepted” manuscripts have been peer-reviewed and accepted for publication. They are posted online prior to technical editing, formatting for publication and author proofing. The American Chemical Society provides “Just Accepted” as a service to the research community to expedite the dissemination of scientific material as soon as possible after acceptance. “Just Accepted” manuscripts appear in full in PDF format accompanied by an HTML abstract. “Just Accepted” manuscripts have been fully peer reviewed, but should not be considered the official version of record. They are citable by the Digital Object Identifier (DOI®). “Just Accepted” is an optional service offered to authors. Therefore, the “Just Accepted” Web site may not include all articles that will be published in the journal. After a manuscript is technically edited and formatted, it will be removed from the “Just Accepted” Web site and published as an ASAP article. Note that technical editing may introduce minor changes to the manuscript text and/or graphics which could affect content, and all legal disclaimers and ethical guidelines that apply to the journal pertain. ACS cannot be held responsible for errors or consequences arising from the use of information contained in these “Just Accepted” manuscripts.

1
2
3
4
5
6
7
8
9
10
11
12
13
14
15
16
17
18
19
20
21
22
23
24
25
26
27
28
29
30
31
32
33
34
35
36
37
38
39
40
41
42
43
44
45
46
47
48
49
50
51
52
53
54
55
56
57
58
59
60

Analysis of Proline Substitutions Reveals the Plasticity and Sequence Sensitivity of Human IAPP Amyloidogenicity and Toxicity

Zachary Ridgway⁽¹⁾, Charles Eldrid⁽²⁾, Alexander Zhyvoloup⁽²⁾, Aisha Ben-Younis⁽²⁾, Daeun Noh⁽³⁾, Konstantinos Thalassinos^{(2)*}, and Daniel P. Raleigh^{(1,2)*}

⁽¹⁾ Department of Chemistry, Stony Brook University, Stony Brook, NY 11794-3400, USA

⁽²⁾ Institute of Structural and Molecular Biology, University College London, Gower Street, London, WC1E 6BT

⁽³⁾ Graduate Program in Biochemistry and Structural Biology, Stony Brook University, Stony Brook, NY 11794-3400, USA

* Authors to whom correspondence should be addressed

Daniel Raleigh

Email: Daniel.raleigh@stonybrook.edu or draleigh@ucl.ac.uk

Phone +1 631 632 9547 or +44 (0)20 7679 2000

Konstantinos Thalassinos

Email: k.thalassinos@ucl.ac.uk

Phone +(44) 02076792197

Key words: Amylin, Amyloid, Ion Mobility Mass Spectrometry, Islet Amyloid Polypeptide, Metabolic Disease, Type 2 Diabetes

Running Title: Sequence Sensitivity of IAPP amyloid formation and toxicity

ABSTRACT

Pancreatic amyloid formation by the polypeptide IAPP contributes to β -cell dysfunction in type 2 diabetes. There is a one-to-one correspondence between the ability of IAPP from different species to form amyloid *in vitro* and the susceptibility of the organism to develop diabetes. Rat IAPP is non-amyloidogenic and differs from human IAPP at six positions, including three proline replacements: A25P, S28P, S29P. Incorporation of these proline residues into human IAPP leads to a non-amyloidogenic analogue which is used clinically. The role of the individual proline residues is not understood. We examine the three single and three double proline substitutions in the context of human IAPP. An S28P substitution significantly decreases amyloidogenicity and toxicity, while an S29P substitution has very modest effects despite being an identical replacement just one residue away. The consequences of the A25P substitution are between those of the two Ser to Pro substitutions. Double analogs containing an S28P replacement are less amyloidogenic and less toxic than the IAPP_{A25P S29P} double analog. Ion mobility mass spectrometry reveals that there is no correlation between monomer or dimer conformation as reported by collision cross sections measurements and the time to form amyloid. The work reveals both the plasticity of IAPP amyloid formation and the exquisite sequence sensitivity of IAPP amyloidogenicity and toxicity. The study highlights the key role of the S28P substitution and provides information that will aid the rational design of soluble variants of IAPP. The variants studied here offer a system to further explore features which control IAPP toxicity.

Abbreviations:

CCS, collision cross section; EC_{50} , the concentration required to achieve 50% of the effective in a IAPP toxicity assay; Fmoc, Fluorenylmethyloxycarbonyl; HPLC, high performance liquid chromatography; hIAPP, human islet amyloid polypeptide; rIAPP, rat islet amyloid polypeptide; IAPP_{A25P}, an A25P analog of hIAPP; IAPP_{S28P}, an S28P analog of hIAPP; IAPP_{S29P}, an S29P analog of hIAPP; IAPP_{A25P S28P}, an A25P S28P analog of IAPP; IAPP_{A25P S29P}, an A25P S29P analog of IAPP; IAPP_{S28P S29P}, an S28P S29P analog of IAPP; IM-MS, ion-mobility mass spectrometry; IWS_D_{CCS}, the intensity weighted standard deviation of the CCS distribution; SASA, solvent accessible surface area; TEM, transmission electron microscopy; T_{50} , the time required to reach half the maximum thioflavin-T fluorescent intensity; ThT, thioflavin-T.

INTRODUCTION

More than 30 human diseases, including Alzheimer's disease and type 2 diabetes, involve the misfolding of normally soluble proteins into β -sheet rich amyloid fibrils¹⁻³. In type 2 diabetes, the neuropancreatic hormone islet amyloid polypeptide (IAPP, also known as amylin) aggregates to form amyloid deposits in the islets of Langerhans. IAPP is synthesized in the pancreatic β -cells and co-secreted with insulin in response to the same stimuli⁴⁻⁷. IAPP normally works in concert with insulin to regulate glucose metabolism and energy storage, but aggregates by an unknown mechanism in type 2 diabetes. Although IAPP amyloid formation is not believed to be the cause of type 2 diabetes, it contributes to β -cell death and dysfunction in the disease and has been shown to be a critical contributor to the failure of islet transplants^{5, 7-14}. Type-1 diabetes involves the destruction of the β -cells and thus insulin and IAPP have traditionally been thought to be absent in the disease. However, recent work reveals that some β -cells remain in the early stages of some forms of type-1 diabetes and IAPP amyloid formation has been suggested to contribute to the loss of β -cells in type-1 diabetes¹⁵⁻¹⁷.

Not all species develop type 2 diabetes, and not all species form islet amyloid *in vivo*¹⁸⁻²¹. To date, there is a one-to-one correlation between the *in vitro* amyloidogenicity of an IAPP sequence and whether an organism develops type 2 diabetes. Mouse and rat IAPP (rIAPP) have identical sequences and are not amyloidogenic *in vitro*, except at very high concentrations. Neither rats nor mice develop type 2 diabetes, nor are there any reports of islet amyloid in non-transgenic rats or mice, although rats and mice transgenic for hIAPP develop islet amyloid and type 2 diabetes^{7, 21-23}. The rodent sequences differ from human IAPP (hIAPP) at only six positions: H18R, F23L, A25P, I26V, S28P, and S29P (Figure 1). The F23L mutation has only a modest impact on hIAPP amyloid formation and the I26V substitution is very conservative.

Particular attention has been focused on the three proline residues and an IAPP analog containing these three substitutions (Pramlintide, also known as Symlin) has been approved for clinical use^{24, 25}. Pramlintide is non-toxic and is not amyloidogenic except at very high concentrations, far above those used clinically or used for formulation²⁶. However, it is not known if each of the prolines make similar contributions to the lack of amyloidogenicity and cytotoxicity of Pramlintide and rIAPP.

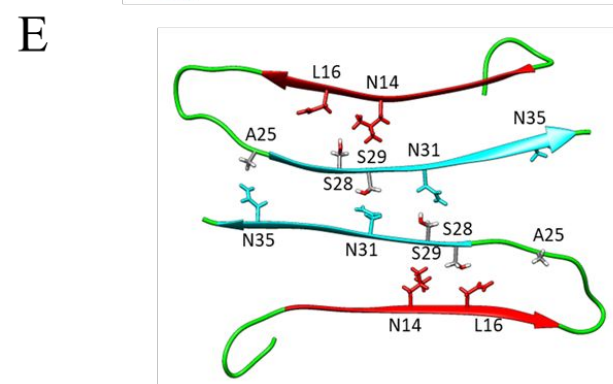
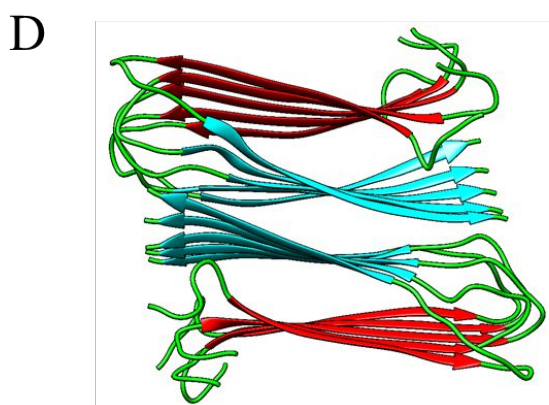
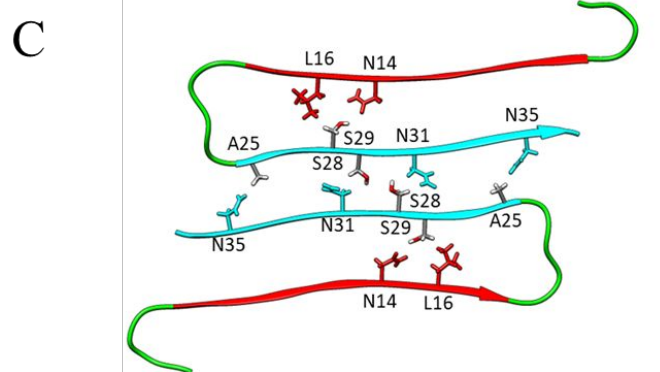
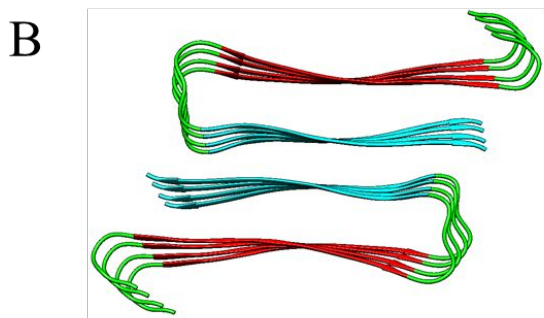


Figure 1. Primary sequence of IAPP and structure of the human IAPP amyloid fibril. **(A)** Comparison of human IAPP (hIAPP) and rat IAPP(rIAPP) primary sequences. Both polypeptides contain a disulfide bond between residues Cys2 and Cys7, and an amidated C-terminus. Residues in rat IAPP which differ from those in human IAPP are depicted in red. **(B)** Top down view of a ribbon structure of the high resolution model of the human IAPP fibril, based on X-ray crystal β -strand structures of IAPP fragments²⁷. The N-terminal β -strand is

1
2
3 colored red, and the C-terminal cyan. The N-terminal seven residues which are not believed to
4 participate in the fibril core, as well as the less ordered loop region from residues 18-24 are
5 colored green. **(C)** Top view of one layer of the fibril structure based on crystal structures of
6 hIAPP fragments²⁷. **(D)** Top down view of a ribbon structure of the high resolution model of the
7 human IAPP fibril, based on solid state NMR studies. **(E)** Top view of one layer of the fibril
8 structure based on solid state NMR studies²⁸. Residues 25, 28, 29 as well as residues that pack
9 against them are shown in stick format.
10
11
12
13

14 While Pramlintide is approved for clinical use, it still suffers from solubility issues and
15 cannot be co-formulated with commercial insulin formulations. This has generated considerable
16 interest in the design of next generation analogs of human IAPP (hIAPP)^{5, 20}. Deducing the
17 relative importance of each proline replacement will aid in the design process and will also
18 provide important clues about the factors which control amyloidogenicity and toxicity.
19
20
21
22
23
24

25 In this work we analyze the roles of each individual proline substitution and all double
26 proline analogs. The work reveals both the plasticity of IAPP amyloid formation and remarkable
27 sequence specific effects. Striking differences between the effects of an S28P and S29P
28 substitution on amyloidogenicity and toxicity are observed. The effects of the A25P replacement
29 lie between those of the two Ser to Pro replacements. Double analogs containing an S28P
30 substitution are less amyloidogenic and less toxic than the IAPP_{A25P S29P} double analog. The data
31 reveals the sequence sensitivity of IAPP amyloidogenicity and toxicity and highlights the key
32 role of the S28P substitution. Previous studies have revealed sequence specificity in hIAPP
33 involving the Asn residues. Asn21 and Asn22 exhibit sequence specificity with Asp
34 substitutions, where the substitutions result in a non-aggregating (N21D) and amyloidogenic
35 (N22D) variant²⁹. Asn to Leu substitutions at positions 21 and 22 have also shown similar
36 specificity³⁰.
37
38
39
40
41
42
43
44
45
46
47
48
49
50
51
52

53 The data set described in this work also provides a test of algorithms developed to
54 correlate amyloidogenicity and sequence. The details of the rank order of the time to form
55
56
57

1
2
3 amyloid is not predicted by many of the popular methods used to analyze amyloidogenicity. Ion-
4
5 mobility mass spectrometry (IM-MS) is employed to probe the conformational propensities of
6
7 the various peptides in order to test if there is a correlation between conformational properties of
8
9 monomers, dimers and amyloidogenicity. No significant conformational differences are observed
10
11 at the level of the collision cross sections (CCS) for a given oligomer charge state between the
12
13 different variants.
14
15
16
17
18

19 **MATERIALS AND METHODS**

20 **Peptide Synthesis and Purification**

21
22 Human IAPP (UniProtKB P10997) and the six proline variants were synthesized on a 0.10 mmol
23
24 scale using 9-Fluorenylmethyloxycarbonyl (Fmoc) chemistry with a CEM Liberty Blue peptide
25
26 synthesizer. Fmoc-PAL-PEG-PS resin (0.18mmol/eq) was used to afford a C-terminal amide.
27
28 Pseudoproline derivatives were used as previously described to prevent aggregation during
29
30 synthesis^{31, 32}. The first residue attached to the resin, beta branched amino acids, arginine, and all
31
32 pseudoproline dipeptide derivatives were double coupled. A trifluoroacetic acid (TFA) based
33
34 cocktail (92.5% TFA, 2.5% triisopropylsilane, 2.5% 3,6-Dioxa-1,8-Octanedithiol, and 2.5% H₂O
35
36 (%v/v)) was used to cleave synthesized peptides from the resin and scavenge side chain
37
38 protecting groups. Crude peptides were dissolved in 20% acetic acid (4 mg/ml) and lyophilized.
39
40 Peptides were oxidized to form a disulfide bond between residues Cys2 and Cys7 in 100%
41
42 dimethyl sulfoxide (DMSO) at a concentration of 10mg/ml on a shaker at room temperature for
43
44 three days. Peptides were purified using reverse-phase HPLC (RP-HPLC) (Higgins Analytical
45
46 C18 preparative column, 25mm x 250mm), utilizing a gradient elution composed of buffer A
47
48 (100% H₂O and 0.045% HCl) and buffer B (80% Acetonitrile, 20% H₂O, and 0.045% HCl).
49
50
51
52
53
54
55
56
57
58
59
60

1
2
3 Purified peptides were lyophilized. HCl was used as a counterion instead of TFA, as TFA can
4 affect the rate of amyloid formation as seen in thioflavin-T kinetic assays and can affect cell
5 toxicity experiments³³. A second HPLC purification was used to remove residual cleavage
6 scavengers as well as residual TFA. 1,1,1,3,3,3-hexafluoroisopropanol (HFIP) was used to
7 dissolve dry peptide for the second purification. Matrix assisted laser desorption ionization time-
8 of-flight (MALDI-TOF) mass spectrometry and analytical HPLC were performed to confirm the
9 mass and the purities of the peptides respectively: hIAPP (WT), expected 3903.6, Da observed
10 3904.1 Da; IAPP_{A25P}, expected 3929.4 Da, observed 3930.6 Da; IAPP_{S28P}, expected 3913.4 Da,
11 observed 3914.9 Da ; IAPP_{S29P}, expected 3913.4 Da, observed 3914.8 Da; IAPP_{A25P S28P},
12 expected 3939.4 Da, observed 3937.5 Da; IAPP_{A25P S29P}, expected 3939.4 Da, observed 3941,6
13 Da; IAPP_{S28P S29P}, expected 3923.4 Da , observed; 3924.8 Da.

31 Preparation of Peptide Stock Solutions

32
33 Purified peptides were dissolved in neat HFIP to a target concentration of 0.8 mg/ml and
34 allowed to stand at room temperature for four hours. Peptide stocks were filtered using a 0.22
35 μm Millex low protein binding durapore membrane filter. 10 μL aliquots of stock were
36 lyophilized for 24 hrs and reconstituted in buffer to determine the concentration of the original
37 HFIP stock solution. Concentration was determined using the absorbance at 280 nm. Aliquots
38 for thioflavin-T assays were lyophilized for 24 hrs in order to remove residual HFIP.

49 Fluorescence Assays

50
51 Thioflavin-T kinetic assays were performed to monitor kinetics of amyloid formation using a
52 Molecular Devices SpectraMax Gemini EM microplate reader, measured with 450 nm excitation
53

1
2
3 and 485 nm emission. Experiments were conducted at 25°C without shaking. Peptides were
4 resuspended in 10 mM Phosphate buffer with 140 mM KCl, pH 7.4 Final peptide concentrations
5 were 16 μ M, and the Thioflavin-T concentration was 32 μ M. This chosen concentration of
6 Thioflavin-T has been previously shown to have no effect on the rate of amyloid formation by
7 IAPP^{34, 35}. Samples were loaded in a 96-well clear bottom plate with a non-binding coating and
8 each sample was run in triplicate. Unused wells were filled with buffer and sealing tape was used
9 to prevent evaporation. It has been shown that the rate of sampling can affect the rate of amyloid
10 formation in plate reader experiments³⁶. The effect arises from the different amount and
11 frequency of agitation induced by the movement of the plate reader carriage during sampling.
12 For all ThT assays, all 96 wells were read, with sampling occurring at ten minute intervals.
13
14
15
16
17
18
19
20
21
22
23
24
25
26
27

28 **Transmission Electron Microscopy**

29
30
31 Transmission electron microscopy (TEM) was used to confirm presence or absence of amyloid
32 fibrils. Images were taken at the Life Sciences Microscopy Center at Stony Brook University. 15
33 μ l aliquots taken from ThT kinetic assays at the end of the experiment were loaded on Carbon-
34 coated Formvar 300 mesh copper grid for one minute. The aliquot was blotted and one drop of
35 2% uranyl acetate was placed on the grid for one minute to negatively stain the sample.
36
37
38
39
40
41
42
43
44

45 **Cytotoxicity Assays and Measurement of EC₅₀ Values**

46
47 INS-1 cells were purchased from AddexBio and cultured with optimized RPMI-1640
48 (AddexBio, #C0004-02) medium supplemented with 10% ultra-low IgG FBS (Gibco,
49 #16250078). CellTiter-Glo 2.0 (Promega, #G9242) and CellTox Green (Promega, # G8741)
50 assays were used to evaluate the cytotoxicity of hIAPP and variants towards INS-1 cells. Briefly,
51
52
53
54
55
56
57
58
59
60

1
2
3 the evaluation of cytotoxicity was performed as follows. Cells were seeded at 6,000-7,000 cells
4 per well (~50% confluence) on a 96-well half-area clear bottom white plates (Greiner, #675083)
5
6 and incubated for 36 hrs in 5% CO₂ humidified incubator at 37°C. Serial dilutions of the peptides
7
8 were freshly prepared before use from lyophilized peptide aliquots. Cells were exposed to
9
10 varying concentrations of peptide diluted in fresh complete medium for 24 hrs. For CellTiter-Glo
11
12 2.0 assays, culture plates were cooled to RT and an equal volume of the assay reagent was added
13
14 to the treated cells. The plates were vigorously (700 rpm) shaken for 1 min and luminescence
15
16 intensity was measured using a Clariostar plate reader. For the CellTox Green assay, the cells
17
18 were exposed to the tested peptide in presence of the assay dye (1:5000 dilution) for 24 hrs
19
20 before fluorescence intensity was measured (480 nm excitation and 525 nm emission). Statistical
21
22 analysis and calculation of EC₅₀ values were completed using Graph Pad Prism 5.
23
24
25
26
27
28
29
30

31 **Ion Mobility Mass Spectrometry (IM-MS)**

32
33 Lyophilized peptides were dissolved in 100 % LC-MS grade DMSO at a concentration of 3.2
34
35 mM and incubated for 24 hrs at room temperature. Samples were directly infused into a Synapt
36
37 G1 (waters Corp, UK). Prior to direct infusion samples were diluted 100-fold using 100 mM
38
39 ammonium acetate pH 7.5. The 350-5000 *m/z* range was calibrated using cesium iodide clusters
40
41 in water. Collision cross section (CCS) calibration was performed on the day of data collection,
42
43 using a mixture of synthetic homopolymer poly-ethylene oxide (PEO) (5M PEO, 10M NaCl in
44
45 LC-MS grade methanol) and peptides from equine cytochrome C digested by trypsin (0.5 mg/ml
46
47 in 49/49/2 (v/v) % of water/methanol/acetic acid solution)³⁷⁻³⁹. CCS calibration was performed
48
49 as previously described (Figure S4-S6)⁴⁰. Peak top values were initially picked manually and
50
51 converted into CCS values. In addition, a Python script was written in order to find peak tops by
52
53
54
55
56
57
58
59
60

1
2
3 relative maxima and convert arrival time into CCS and, in order to accelerate data analysis.

4
5 Comparison of monomer and dimer populations were performed by fitting populations using
6
7 FitYK. Reported CCS values are calculated from reduced mobilities in nitrogen, using helium
8
9 CCS calibrant values, or $^{TW}CCS_{N_2 \rightarrow He_2}$, according to recently published recommendations⁴¹.

10
11
12 Measurements were performed in triplicate on different days.

13 14 15 16 17 **Photoinduced Crosslinking Studies**

18
19 Photochemical induced crosslinking of unmodified proteins (PICUP) was performed as
20
21 previously described¹². Peptides were cross linked using Tris(bipyridyl)Ru(II) in the presence of
22
23 ammonium persulfate. Peptides were reconstituted in pH 7.4 PBS and centrifuged at 18,000g for
24
25 five minutes For a given reaction, 15 μ L of 40uM peptide was mixed with 2.5 μ L of Ru(II), 2.5 μ L
26
27 APS, and quenched with a 10uL aliquot of sample buffer with 5% beta-mercaptoethanol. Final
28
29 relative molar concentrations of reagents were 1 / 3.5 / 70 peptide / Ru(II) / APS. After the
30
31 reaction was quenched, the quenched samples were placed on a heat block at 90°C for five
32
33 minutes prior to loading. A 10-20% acrylamide Tris / Tricine gradient gel was used to separate
34
35 oligomeric species, visualized using silver staining (SilverXpress, Invitrogen). Densitometry was
36
37 carried out using gelanalyzer2010a software.
38
39
40
41
42
43
44
45
46

47 **Fractional SASA Calculations**

48
49 The fractional solvent accessible surface area (SASA) of residues of interest were determined
50
51 using:

$$52$$
$$53 \text{ Fractional SASA} = \frac{\text{SASA (Fibril)}}{\text{SASA (Tripeptide)}}$$

54
55
56
57

1
2
3 Tripeptide SASA values were calculated using Maestro (Schrodinger), and sidechain SASA in
4 the fibril models for the Tycko and Eisenberg structures were calculated using VMD. Tripeptides
5 corresponding to residues 24-26, 27-29 and 28-30 of IAPP were constructed in a fully extended
6 conformation for use as a reference state. Fractional SASA values are reported as a range for the
7 Tycko model, as monomers in the fibril layer are not perfectly symmetric.
8
9
10
11
12
13
14
15
16

17 RESULTS

18 **Residues 25, 28 and 29 are found in unique environments in the human IAPP amyloid** 19 **fibril**

20
21
22 Two high resolution models, based upon experimental data, are available for the human
23 IAPP amyloid fibril; one is based on X-ray structures of small peptide fragments of IAPP
24 (Eisenberg model) and the second is based on solid state NMR studies (Tycko model)^{27, 28}.
25
26 Analysis of both models reveals that the site of each proline substitution is in a unique
27 environment in the amyloid fibril.
28
29
30
31
32
33

34 The two models share many common features, but do have some differences. Both agree
35 that each layer of a fibril filament is composed of two U-shaped IAPP monomers in a symmetric
36 structure, with no intra-peptide backbone hydrogen bonding (Figure 1). Backbone hydrogen
37 bonds are formed between adjacent IAPP molecules in the same stack, while sidechain-sidechain
38 hydrogen bonds and tight packing of sidechains occurs between the two adjacent stacks. There
39 are no backbone hydrogen bonds between the two symmetry related stacks. The interface
40 between the two columns is tightly packed and, in the X-ray based model, encompasses residues
41 23 to 37 (Figure 1). The Tycko model defines the two β -strands as being composed of residues 8
42 to 17 and 26 to 36 while the Eisenberg model, based on peptide crystal structures, orders the
43 strands from residue 7 to 18 and 25 to 36 respectively. A25 is located at the start of the second
44
45
46
47
48
49
50
51
52
53
54
55
56
57
58
59
60

1
2
3 β -strand in the Eisenberg model and projects outwards in proximity to N35 of the other IAPP
4 monomer in the same layer and L27 of the same monomer. In the Tycko model, A25 is in the
5 partially disordered loop region, but in proximity to N14 and L16 of the same IAPP monomer.
6
7 A25 lies at the interface between the two stacks rather than in the interior of a stack. In both
8 models, S28 and S29 are located in the C-terminal β -strand. S28 projects towards the N-terminal
9 strand of the same monomer, in proximity to L12 and A14 and T30 and is buried with the core of
10 the stack. The neighboring S29 residue projects outward from the stack and makes contacts with
11 residues in the other monomer in the stack, including S29 and N31 located in the C-terminal β -
12 strand of the neighboring IAPP monomer. S29 is part of the steric zipper interface in the
13 Eisenberg model. Thus S29, like A25, is an interfacial residue (Figure-1). The S28 and S29
14 sidechains in a given peptide also form a network of interactions with the same residue in chains
15 immediately above and below in the same stack. These are reminiscent of the network of
16 interactions formed by Asn and Gln sidechains which are thought to stabilize amyloid fibers^{42, 43}.
17
18 The fractional solvent accessibility of the A25, S28 and S29 sidechains in the fibril were
19 calculated, defined relative to a tripeptide with composition corresponding to the local sequence
20 in an extended conformation. A25 is 2% to 9% exposed in the Tycko model, and 0% in the
21 Eisenberg model. The fractional solvent accessibility of the S28 and S29 sidechains are 1% to
22 30% and 8% to 18% respectively in the Tycko model and 2% and 0% respectively in the
23 Eisenberg model. All three residues populate the allowed regions of the Ramachandran plot.
24
25
26
27
28
29
30
31
32
33
34
35
36
37
38
39
40
41
42
43
44
45
46
47
48
49

50 **Design of IAPP variants to study the of role proline substitutions in rIAPP**

51 A library of peptides was synthesized to study the role that each proline substitution
52 found in rIAPP plays in mitigating amyloidogenicity and β -cell cytotoxicity. Three variants were
53 prepared with each of the single proline substitutions found in rIAPP (IAPP_{A25P}, IAPP_{S28P},
54
55
56
57
58
59
60

1
2
3 IAPP_{S29P}), as well as three variants encompassing all possible permutations of double proline
4
5 substitutions (IAPP_{A25P S28P}, IAPP_{A25P S29P}, IAPP_{S28P S29P}).
6
7
8
9

10 **Proline substitutions have strikingly different effects and the S28P substitution has the** 11 **largest impact on amyloid formation** 12

13 The time course of amyloid formation was determined using fluorescence monitored
14 thioflavin-T (ThT) binding assays. ThT is an extrinsic dye whose fluorescence increases upon
15 binding to amyloid fibrils. This dye provides a convenient method to follow amyloid formation,
16 but can lead to false positive and negative results in some cases^{44, 45}. However, ThT assays have
17 been shown to reliably report on the time course of hIAPP amyloid formation under the
18 conditions of our studies³⁵. There is no clear relationship between the intensity of the ThT signal
19 and the quantity of amyloid fibrils formed as mutations or changes in solution conditions may
20 alter the affinity of the dye for the fibrils, or alter the lateral association of proto-fibrils and fibrils
21 which, in turn, could lead to differing amounts of fibril surface exposed for dye binding. In
22 addition, the dye may bind in subtly different conformations to different amyloid fibrils which
23 could impact its quantum yield. Thus, we do not interpret the final ThT fluorescence intensities
24 quantitatively and TEM was used to confirm the presence or absence of amyloid fibrils in every
25 sample.
26
27
28
29
30
31
32
33
34
35
36
37
38
39
40
41
42

43 Several of the variants studied showed ThT curves indicative of typical amyloidogenic
44 proteins, while others did not display any gain in fluorescence signal over the time course of the
45 study (one week). Both the A25P and S29P formed amyloid as judged by TEM and ThT assays
46 even though both residues participate in the interface between the two stacks of monomers in the
47 fiber.
48
49
50
51
52
53
54
55
56
57
58
59
60

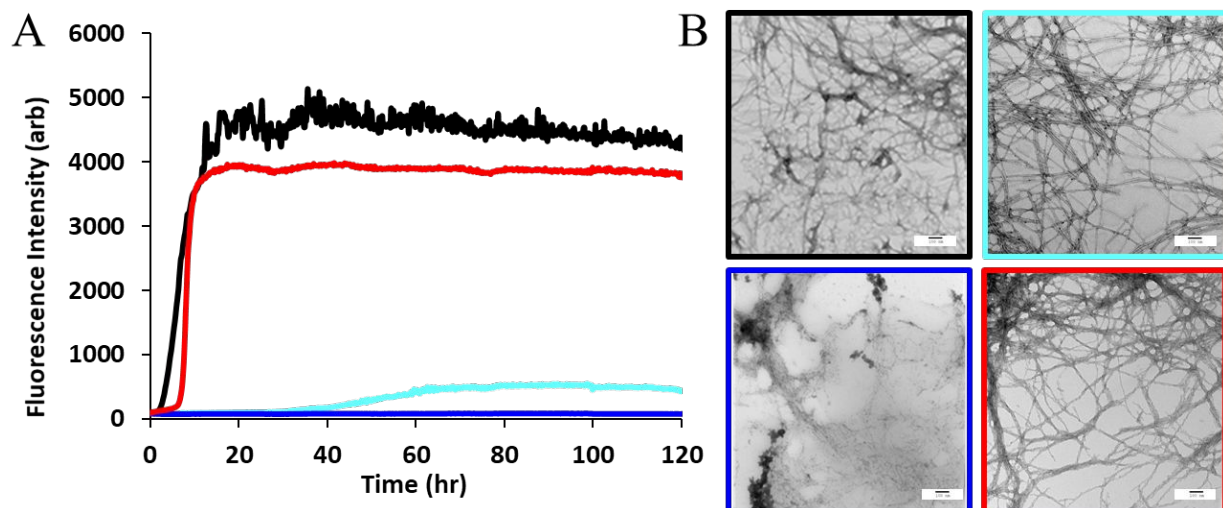


Figure 2. The S28P substitution has a dramatic effect upon amyloid formation by hIAPP (A) Time dependence of amyloid formation hIAPP and single proline variants in PBS. monitored by ThT fluorescence. hIAPP (black); IAPP_{A25P} (cyan); IAPP_{S28P} (blue); IAPP_{S29P} (red). (B) TEM images of hIAPP (black), and IAPP_{A25P} (cyan), IAPP_{S28P} (blue), IAPP_{S29P} (red). Aliquots for TEM were collected at the conclusion of the ThT experiments. Assays were conducted with 16μM peptide, 32 μM ThT, at pH 7.4 10 mM phosphate, 140 mM KCl, 25°C. Scale bars in TEM images are 100 nm.

Striking differences were observed between the effects of a Ser to Pro replacement at positions 28 and 29. Under the conditions studied, hIAPP as well as IAPP_{A25P} and IAPP_{S29P} showed an increase in ThT fluorescence over the time course of the studies, but IAPP_{S28P} did not. Wild type hIAPP and IAPP_{S29P} aggregated appreciably faster than IAPP_{A25P}, as determined by T_{50} , the time required to reach half the maximum ThT fluorescent intensity. IAPP_{S29P} aggregated on a time scale comparable to hIAPP, with a T_{50} of 6.7 ± 0.4 hours, compared to the T_{50} value of 6.4 ± 1.6 for hIAPP. IAPP_{A25P} formed amyloid more slowly having a T_{50} value of 42.8 ± 0.5 hours. The S28P substitution had the most dramatic effect and IAPP_{S28P} did not show an increase in ThT fluorescence during the full seven days of the kinetic experiment. TEM imaging confirmed the presence of fibrils in all samples that were found to be amyloidogenic by ThT assays and confirmed their absence in the IAPP_{S28P} sample. Some of the EM grids contained material which could result from amorphous aggregates. We were unable to detect any differences in fibril

1
2
3 morphology at the level of the TEM images among those samples which did form amyloid. The
4 final ThT intensity observed for the IAPP_{A25P} sample was noticeably less than that observed for
5 hIAPP or for the S29P analog. However dense mats of typical amyloid fibrils were clearly
6 visible in the TEM images of the IAPP_{A25P} sample (Figure 2). The reason(s) for the differences
7 in final ThT intensity are not known and, for the reasons outlined above, we believe it is
8 problematic to speculate on their origin. Nonetheless, the key observation is that behavior of the
9 A25P variant lies between that of the S28P and S29P analogs. The rank order of the effect of the
10 analogs upon amyloid formation was S28P>A25P >> S29P. The reduced final ThT intensity for
11 the A25P variant suggests that the fibril superstructure is different for this analog and that these
12 changes lead to either reduced ThT binding or to a change in the structure of the bound ThT that
13 reduces its quantum yield.
14
15
16
17
18
19
20
21
22
23
24
25
26
27
28
29

30 Of the variants containing two Pro substitutions, IAPP_{A25P S29P} was the only one to show
31 an increase in ThT fluorescence for experiments conducted at 16 μ M peptide concentration, with a
32 T_{50} value of 16.2 ± 1.0 hours. TEM imaging confirmed the presence of amyloid fibrils formed by
33 this peptide. Variants containing the S28P substitution (IAPP_{A25P S28P} and IAPP_{S28P S29P}) showed
34 no increase in ThT fluorescence over the one week course of these studies, and amyloid was not
35
36
37
38
39
40
41
42
43
44
45
46
47
48
49
50
51
52
53
54
55
56
57
58
59
60

detected in TEM samples from these samples (Figure 3).

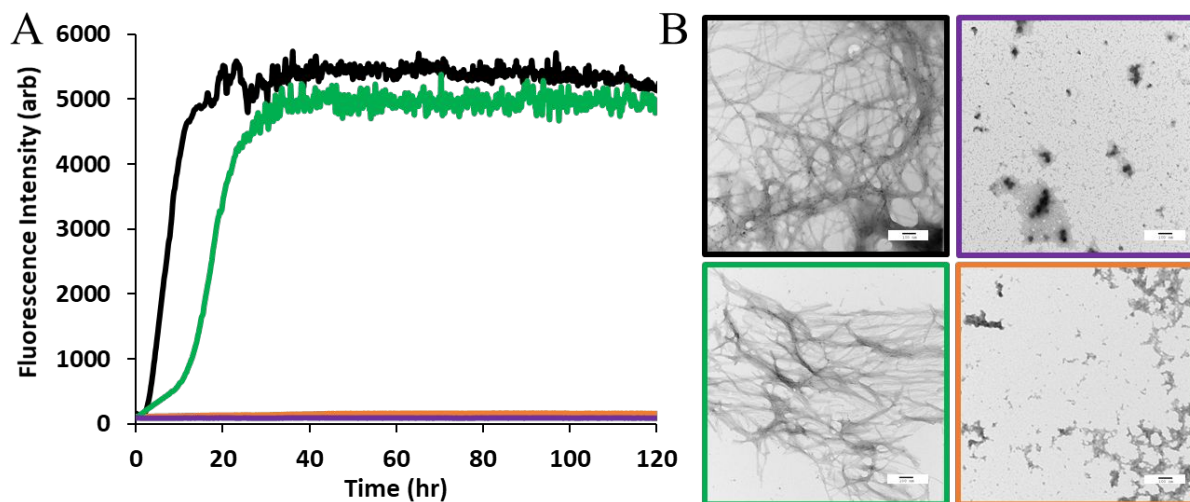


Figure 3. Double proline variants which contain an S28P substitution are significantly less amyloidogenic. **(A)** Time dependence of amyloid formation hIAPP and double proline variants in PBS, monitored by ThT fluorescence. hIAPP (black), IAPP_{A25P S28P} (purple), IAPP_{A25P S29P} (green), and IAPP_{S28P S29P} (orange). **(B)** TEM images of hIAPP (black), IAPP_{A25P S28P} (purple), IAPP_{A25P S29P} (green), and IAPP_{S28P S29P} (orange). Aliquots for TEM were collected at the conclusion of the ThT experiments. Assays were conducted using the following conditions: 16 μ M peptide, 32 μ M ThT, pH 7.4 10mM phosphate, 140 mM KCl, 25°C. Scale bars in TEM images are 100 nm.

These results, together with the studies of the IAPP_{S28P} variant, clearly show that the S28P mutation plays the largest role in mitigating hIAPP amyloidogenicity. All variants which lack the S28P mutation have T_{50} values within 6.7-fold of human IAPP under the conditions of our experiments.

The rate of amyloid formation is concentration dependent, thus variants that did not show an increase in ThT fluorescence at 16 μ M peptide concentration were examined at a higher peptide concentration (100 μ M) in an effort to detect amyloid formation. (Figure S1). Under these conditions, IAPP_{S28P} has a T_{50} $7.1 \pm .3$ hours, and IAPP_{A25P S28P} 13.4 ± 1.2 hours (Table 1).

Table 1. Summary of measured T_{50} values for wild type hIAPP and analogues. Data was collected for 16 μ M peptide at 25°C in PBS (pH 7.4).

Peptide	T_{50} (hrs) \pm Std. Dev.
hIAPP	6.4 \pm 1.6
IAPP _{A25P}	42.8 \pm 0.5
IAPP _{S28P}	N/A
IAPP _{S29P}	6.7 \pm 0.4
IAPP _{A25P S28P}	N/A
IAPP _{A25P S29P}	16.2 \pm 1.0
IAPP _{S28P S29P}	N/A

IAPP_{S28P S29P} still did not show an appreciable increase in ThT fluorescence over the time course of the experiment. TEM imaging confirmed the presence of fibrils in the high concentration IAPP_{S28P} and IAPP_{A25P S28P} samples. Multiple kinetic curves from samples run in triplicate are shown in the supporting information (Figure S2), along with plots that include expanded x-axes for the amyloid forming proline variants. The final ThT fluorescence values at saturation and slope of the curves at the midpoint(T_{50}) are provided in the supporting information.

Algorithms designed to predict amyloidogenicity capture general trends of proline substitution effects, but not the details.

A number of algorithms have been developed to predict amyloidogenicity, based on different physiochemical features of polypeptides, or based on the predicted ability of sequences to form steric zipper segments⁴⁶⁻⁵⁰. The seven variants studied here, wild type and the six analogs, provide an opportunity to examine the applicability of these methods to predict the relative time course of amyloid formation by IAPP variants. The analogs form an interesting test

case since they contain similar mutations and, in some cases, involve Ser to Pro substitutions one residue apart. We used five popular methods to compared hIAPP and the set of analogs.

The computational methods chosen show clear differences in the predicted amyloidogenic regions of the proline analogs when compared to the wild type sequence. ZipperDB, which uses a six residue sliding window to evaluate fragments that have the potential to form steric zippers, indicates that proline substitutions significantly disrupt steric zipper propensity in the 20-29 region (Table 2, Figure S3)⁴⁶.

Table 2. Relative predicted amyloidogenicity of hIAPP and variants as determined by various computational algorithms and by ThT kinetic assays.

<i>Method</i>	<i>Least amyloidogenic</i> → <i>Most amyloidogenic</i>
AGGRESCAN	A25P S28P = A25P S29P < A25P < S28P S29P < S28P = S29P < hIAPP
WALTZ	A25P S28P = A25P S29P = A25P < S28P S29P = S28P = S29P < hIAPP
TANGO	A25P S28P = A25P S29P = A25P = S28P S29P = S28P < S29P < hIAPP
PASTA	A25P S28P = A25P S29P = A25P < S28P S29P = S28P = S29P < hIAPP
ZipperDB	A25P S29P < A25P S28P < S28P S29P < S28P < S29P < A25P < hIAPP
Experimental (ThT assay)	S28P S29P < A25P S28P = S28P < A25P < A25P S29P < S29P = hIAPP

In contrast, the wild type sequence exhibits the strongest scoring in the 20-29 region. While this method predicts that any of the proline substitutions diminishes the ability to form steric zippers, the results did not correlate with the trends observed in the kinetic assays. IAPP_{S29P} was predicted by ZipperDB to have the largest effect of the single proline variants in diminishing steric zipper formation, yet IAPP_{S29P} aggregates at a rate similar to hIAPP. WALTZ is a program that predicts amyloidogenic regions of peptides⁴⁷. For hIAPP, WALTZ predicts the 22-29 region to be amyloidogenic. For IAPP_{S28P}, IAPP_{S29P}, and IAPP_{S28PS29P}, WALTZ indicates the 22-27 region is amyloidogenic (Table 2, Table S1). For all variants containing the A25P substitutions,

1
2
3 WALTZ does not predict any amyloid forming region in the peptide. Overall, WALTZ suggests
4 that the A25P substitution will have a larger effect than either of the Ser to Pro substitutions.
5
6 TANGO is a method that predicts amyloidogenicity by determining the likelihood of β -sheet
7 formation⁴⁸. TANGO predicts that all proline substitutions will be less amyloidogenic than
8 hIAPP (Table 2, Table S2), with the A25P and S28Preplacement predicted to have a larger
9 effect than a S29P substitution. hIAPP is predicted by TANGO to have the highest propensity to
10 form amyloid, with S29P hIAPP scoring only slightly lower. Both PASTA and AGGRESCAN
11 predict that the A25P replacement will have the largest effect on amyloid formation (Table 2,
12 Table S3, Table S4). PASTA is based on evaluating pairwise amino acid contacts within the
13 peptide, in the framework of favorable pairwise interactions that lead to increased stability of
14 beta sheets⁴⁹. AGGRESCAN identifies amyloid forming regions based on the amyloidogenic
15 propensity of individual amino acids⁵⁰. Both methods predict that each of the proline variants are
16 less amyloidogenic than hIAPP. However, PASTA and AGGRESCAN rank the S28P-hIAPP
17 and S29P-hIAPP analogs equally and ranks them as being only slightly less amyloidogenic than
18 hIAPP, in contrast to the experimental kinetic observations.

19
20
21
22
23
24
25
26
27
28
29
30
31
32
33
34
35
36
37
38 In summary, all of the programs examined predicted that any of the three proline
39 substitutions will lead to a reduction in amyloidogenicity compared to hIAPP. However, most
40 programs predict A25P to have the largest impact of any point substitution, whereas kinetic
41 assays show that the S28P substitution has the largest effect. TANGO, PASTA, and
42
43
44
45
46
47
48
49
50
51
52
53
54
55
56
57
58
59
60
AGGRESCAN predict the S29P substitution to have minimal impact on amyloid formation, but
only TANGO predicted the S28P substitution to have a larger effect than S29P. Double proline
substitutions generally ranked less amyloidogenic than single proline substitutions.

The effects of the IAPP analogs on cytotoxicity correlate with their effects on amyloid formation.

Dose response experiments were conducted to monitor the effect of hIAPP and variants on cell viability using two independent assays. INS-1 cells, a standard pancreatic rat β -cell line, were used for these studies. Two assays were used to assess cytotoxicity; The CellTiter-Glo assay measures global cellular ATP levels (Figure 4A, B), while the CellTox Green assay reports on membrane integrity by exposing cells to a dye that crosses the cell membrane of compromised cells and binds to DNA (Figure 4C, D).

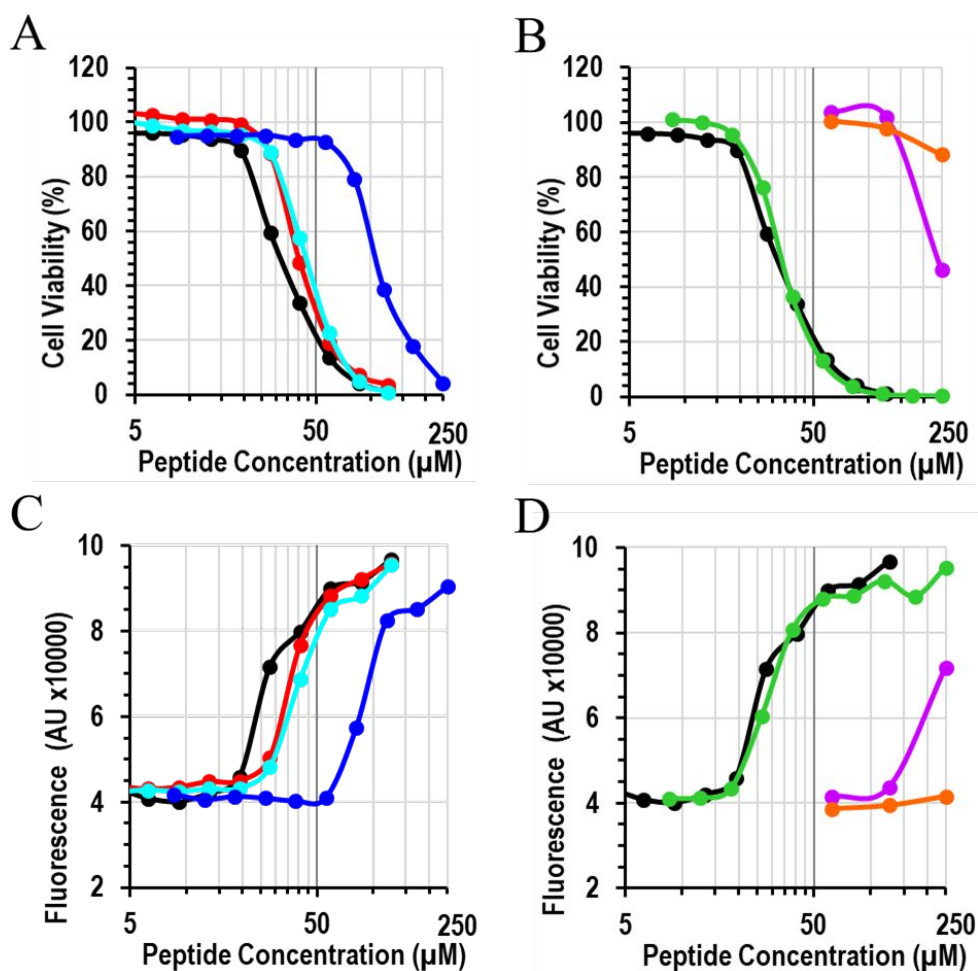


Figure 4. Does-response curves of INS-1 β -cell viability after incubation with hIAPP or variants, as determined by the CellTiter-Glo assay (A, B) and the CellTox Green assay (C, D). hIAPP

(black); IAPP_{A25P} (light blue); IAPP_{S28P} (blue); IAPP_{S29P} (red). IAPP_{A25P S28P} (purple), IAPP_{A25P S29P} (green), and IAPP_{S28P S29P} (orange). The X-axis is plotted on a logarithmic scale.

The effective concentration to generate 50% of the response, EC₅₀, was determined for each peptide using both assays (Table 3).

Table 3. EC₅₀ values (μM) and standard error of the mean (SEM) of hIAPP and variants as judged by CellTiter-Glo and Celltox Green assays. EC₅₀ values were calculated from concentration dependence response curves using PRISM.

	CellTiter-Glo		CellTox Green	
	EC ₅₀ (μm)	SEM	EC ₅₀ (μm)	SEM
hIAPP	48.1	3.3	27.0	2.1
IAPP _{A25P}	61.2	2.0	42.1	5.5
IAPP _{S28P}	164.4	30.8	136.4	8.2
IAPP _{S29P}	53.0	3.9	28.8	2.5
IAPP _{A25P S28P}	N/A ⁽¹⁾	N/A	N/A ⁽¹⁾	N/A
IAPP _{A25P S29P}	46.4	1.3	31.4	5.6
IAPP _{S28P S29P}	N/A ⁽¹⁾	N/A	N/A ⁽¹⁾	N/A

(1) Insufficient toxicity was detected at the highest concentration (300 μM) to allow determination of EC₅₀

hIAPP was toxic to INS-1 cells under all conditions studied, with EC₅₀ values ranging from 27.0 μM to 48.1 μM depending upon the assay used. All single proline variants elicited a cytotoxic response. IAPP_{S28P} was noticeably less cytotoxic than the other single analogs, showing no change in cell viability at concentrations up to 100 μM, while IAPP_{A25P} and IAPP_{S29P} showed stronger effects on cytotoxicity. IAPP_{S28P} had EC₅₀ values approximately four to five-fold higher than hIAPP. Of the double proline analogs, the only variant that showed cytotoxic properties below 150 μM was IAPP_{A25P S29P}. Insufficient toxicity was detected at the highest concentration

1
2
3 (300 μM) to allow determination of the EC_{50} value for the IAPP_{A25P S28P} and IAPP_{S28P S29P} double
4
5 analogs. The CellTox Green assay confirms that a loss of membrane integrity occurs along with
6
7 the metabolic dysfunction detected by the CellTiter-GLO assay. However, the EC_{50} for
8
9 membrane permeabilization occurs at lower peptide concentrations than the EC_{50} values deduced
10
11 from the assays which monitor ATP production.
12
13
14
15
16
17

18 **Ion Mobility Mass Spectrometry analysis shows that there are no significant differences in**
19
20 **the conformations of monomers and dimers based on collision cross section measurements**
21
22

23 It is very difficult to structurally interrogate the species present in solution during amyloid
24
25 formation given their transient nature and polydispersity, so we employed ion mobility-mass
26
27 spectrometry (IM-MS) to probe the conformation of dimers and monomers formed by human IAPP
28
29 and the different variants. IM-MS allows the separation of ions as they travel through a drift tube
30
31 filled with an inert gas, in our case nitrogen. As ions travel through the drift tube, their velocity is
32
33 reduced through collisions with the drift gas. The reduced mobility of ions can be used to calculate
34
35 the collision cross-section (CCS) of the analyte ion and is often expressed in nm^2 or \AA^2 ⁵¹. If protein
36
37 ions of the same mass and charge exhibit different conformations, the one with a more extended
38
39 conformation will experience a greater number of collisions with the gas and have a larger CCS
40
41 than the one with the more compact conformation.
42
43
44
45
46

47 Pioneering IM-MS analysis of IAPP variants and other amyloidogenic proteins has been
48
49 carried out in the past⁵²⁻⁶¹. Previous work has detected differences in conformational behavior and
50
51 stability between human and rat IAPP using IM-MS^{52, 54}. Here we analyzed the tendency of the
52
53
54
55
56
57
58
59
60

IAPP analogs to form lower order oligomers and measured their CCS to explore any relation between conformation and amyloidogenicity and toxicity.

All analogs were found to form a mixture of monomers and dimers (denoted as n^{+z} where n is the oligomeric state and z is the charge, Figure 5, Figure S7).

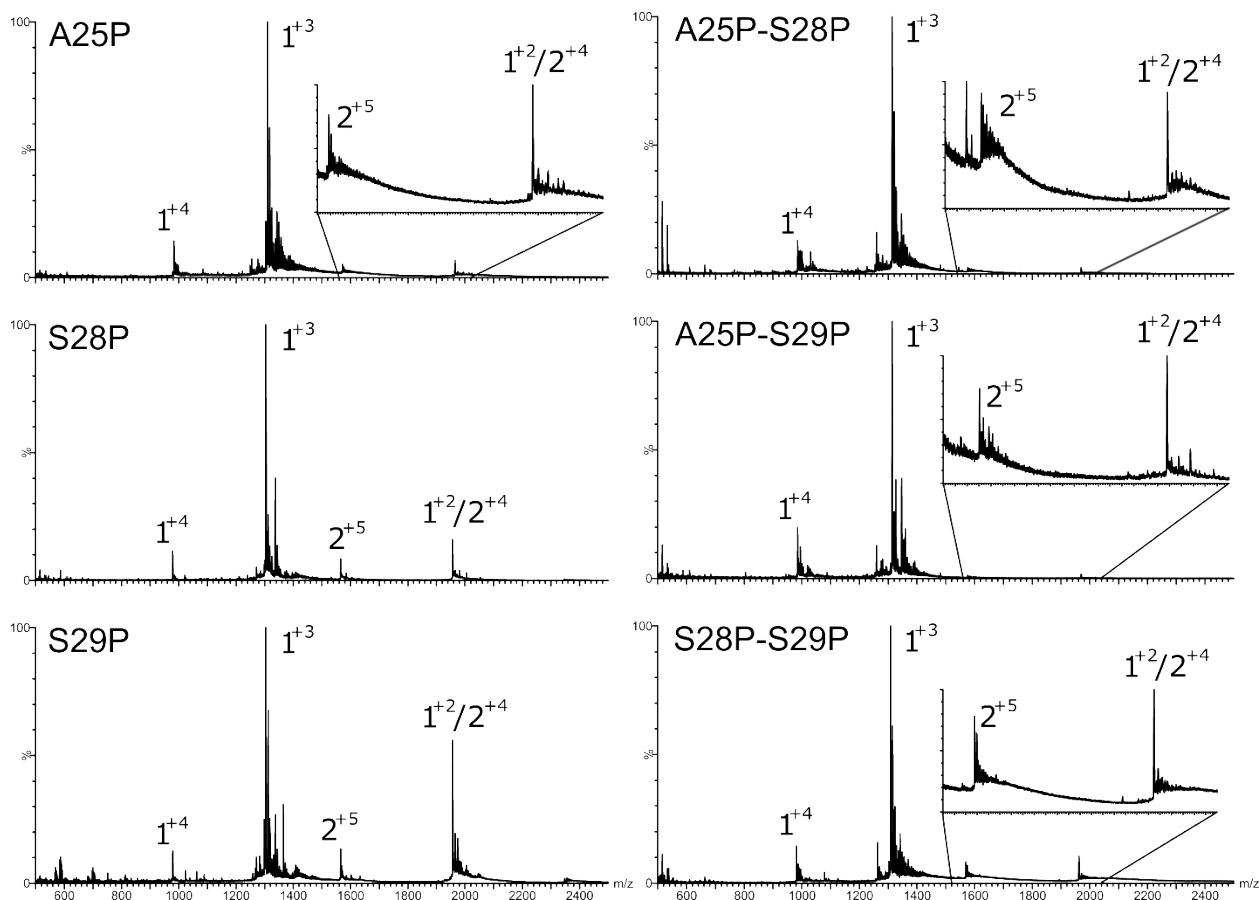


Figure 5. Mass spectra of the proline analogs for IAPP_{A25P}, IAPP_{S28P}, IAPP_{S29P}, IAPP_{A25P S28P}, IAPP_{A25P S29P}, and IAPP_{S28P S29P}, with the species represented as n^{+z} with n being the oligomeric state and z being the charge. Other species with m/z values corresponding to higher order oligomers could be detected at lower intensity, but their charge state and mass could not be unequivocally assigned due to the lack of isotopic peak resolution.

The charge state was calculated for each mobility separated species using their corresponding isotopic peak envelope. m/z values corresponding to higher order oligomeric species could be seen in some cases, but there was not sufficient mass resolution to calculate the charge and hence assign mass. Our spectra are similar to those reported previously, however based on the isotope distributions we assign the species at 1950 m/z as being a mixture of 1^{+2} and 2^{+4} , rather than purely monomeric ^{54-57, 60, 61}. Assigning the oligomer nature of each CCS species was achieved by extracting the corresponding mass spectrum for each species and examining the isotopic spacing in the mass spectrum.

IM-MS analysis showed that all analogs have broadly similar CCSs (Figure 6A), however, there are some differences.

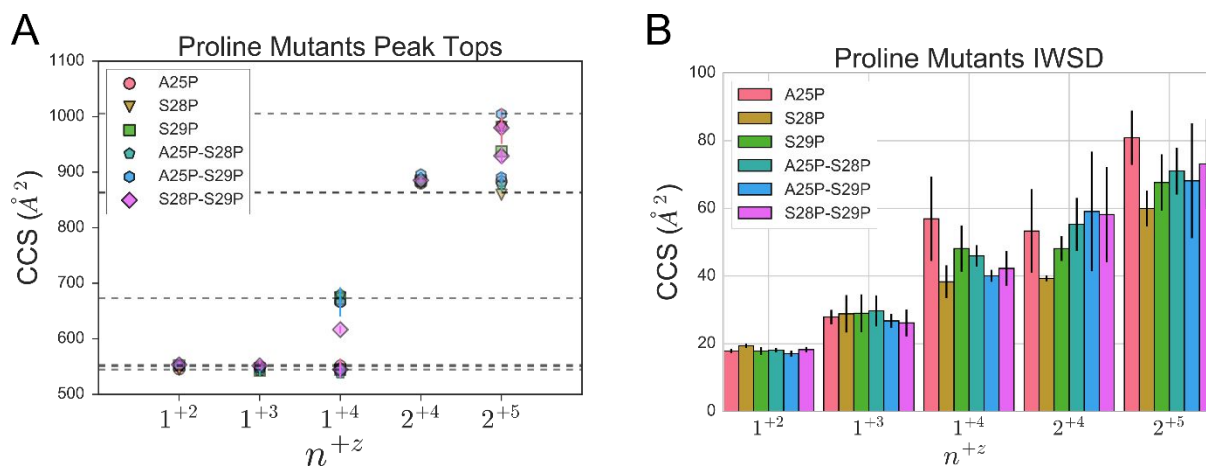


Figure 6. CCS and $IWSD_{CCS}$ values for hIAPP and variants. **A)** Scatter plot of the CCS values of IAPP proline analogs with error bars, with the species represented as n^{+z} , where n is the oligomeric state and z the charge. The horizontal dashed lines correspond to hIAPP CCS values. **B)** Intensity weighted standard deviation of the CCS distribution ($IWSD_{CCS}$).

Two species were observed for the 1^{+4} species for all peptides, however the extended 1^{+4} species formed by IAPP_{S28P-S29P} is more compact (by approximately 8 to 9%) than in other constructs (Table 4).

Table 4. CCS values for IAPP variants in Å². For some ions, two conformations could be detected.

Construct	1^{+2}	1^{+3}	1^{+4}	2^{+4}	2^{+5}
A25P	545.2 ± 4.4	550.0 ± 7.8	666.7 ± 13.1	880.0 ± 2.3	983.1 ± 32.1
			551.7 ± 13.4		883.6 ± 14.6
S28P	544.5 ± 5.2	546.5 ± 5.7	675.0 ± 1.3	881.8 ± 2.1	981.3 ± 3.7
			544.7 ± 14.4		859.5 ± 0.0
S29P	552.5 ± 3.9	542.8 ± 10.5	672.3 ± 4.4	885.1 ± 8.8	937.4 ± 9.1
			544.7 ± 14.4		
A25P-S28P	550.5 ± 3.8	542.9 ± 7.9	680.2 ± 12.7	881.9 ± 2.8	878.5 ± 13.4
			537.7 ± 9.6		
A25P-S29P	551.8 ± 3.1	546.5 ± 4.8	665.9 ± 26.3	896.1 ± 2.3	1004.7 ± 2.9
			544.7 ± 14.4		890.7 ± 10.1
S28P-S29P	553.3 ± 5.9	551.7 ± 8.4	616.6 ± 7.0	885.2 ± 4.6	979.9 ± 10.2
			544.7 ± 14.4		929.3 ± 15.4
hIAPP	544.7 ± 4.6	551.1 ± 8.1	673.0 ± 11.4	864.0 ± 9.9	1005.9 ± 10.4
			552.9 ± 12.2		863.0 ± 21.1

There is no correlation between the CCS values of the extended 1^{+4} species and the EC₅₀ values.

The 2^{+5} state of the IAPP_{S29P} and IAPP_{A25P-S28P} ions occupy single conformations, rather than the two observed for other peptides. Again, there is no clear correlation between CCS values and amyloidogenicity or toxicity for either the 2^{+4} or 2^{+5} species. We also used a metric known as the intensity weighted standard deviation of the CCS distribution (IWSD_{CCS}), which has been used as a complementary statistic to track unfolding in collision induced unfolding experiments and

1
2
3 which provides a simple description regarding the width of a CCS distribution⁶². All monomeric
4 species have similar $IWSD_{CCS}$ values, however the dimers display different behavior (Figure
5 6B), it appears that the $IAPP_{A25P}$ dimer has a wider CCS distribution than the other analogs.
6
7 However, the important point is that we can find no clear relationship between either the CCS
8 values or $IWSD_{CCS}$ of the analogs and propensity to form amyloid fibrils or cellular toxicity.
9
10 Using our assignments of the spectra we compared the area under the curve (AUC) of dimeric vs
11 monomeric populations for the mixed dimeric/monomeric peak (~ 1950 m/z). We find no
12 relationship between either T_{50} or EC_{50} and the relative abundance of dimeric vs monomeric
13 populations for the peptides studied (Figure S8). An avenue for future investigation could
14 involve exploiting new generation, high resolution IM-MS instruments and tandem ion mobility
15 experiments that can further separate sub-populations present in very similar CCS distributions⁶³.
16
17
18
19
20
21
22
23
24
25
26
27
28

29 To complement to these studies, we performed photochemical crosslinking (PICUP) on
30 IAPP using the methods developed by Bitan and Teplow⁶⁴. Previous work performed on hIAPP
31 and non-amyloidogenic rat IAPP showed that rapid oligomerization occurs in solution, with a
32 distribution of monomers to hexamers observed¹². PICUP studies of the proline variants reveals
33 similar features to previous studies of IAPP and non-aggregating IAPP variants (Figure S9).
34 Distributions of oligomeric species are broadly similar for the proline substituted variants, with
35 the exception of $IAPP_{A25P}$, which showed a tendency to occupy lower order oligomers than
36 hIAPP or the other proline variants.
37
38
39
40
41
42
43
44
45
46
47

48 Discussion

49
50 Rat IAPP has been extensively studied as an example of a mammalian IAPP
51 sequence that does not form amyloid or elicit a cytotoxic response in cultured β -cells. The data
52 presented shows that the S28P substitution has the largest impact of the three proline
53
54
55
56
57

1
2
3 substitutions found in rIAPP, in reducing both amyloidogenicity and cytotoxic. In contrast, an
4
5 identical Ser to Pro substitution just one residue away at position 29 showed minimal reductions
6
7 in amyloidogenicity and cytotoxicity despite the fact that S29P is located in the interface
8
9 between the two stacks of IAPP molecules in the amyloid fiber and is part of the steric zipper
10
11 interface. The A25P substitution had a prolonged T_{50} relative to wild type, but a modest effect on
12
13 cytotoxicity. The effects of the A25P substitution and the S29P replacement on the time to form
14
15 amyloid is consistent with prior studies conducted at higher concentration that lead to the
16
17 proposal that IAPP amyloid formation involves an on pathway, transient, β -sheet intermediate
18
19 involving the FGAIL region, and possibly more residues^{65, 66}. The transient β -sheet is formed in
20
21 the intermediate, but needs to be disrupted to generate the final fiber structure and the lag time is
22
23 controlled by the conformational transition of this oligomer intermediate into a structure
24
25 compatible with the fiber. Within the context of this model, proline substitutions should
26
27 destabilize the intermediate as they disrupt β -sheet structure. The A25P substitution should
28
29 destabilize this intermediate as it is in the middle of the FGAIL region and thus lead to a longer
30
31 lag time if the intermediate is on pathway. However, the relatively modest effect upon IAPP
32
33 toxicity suggests that the intermediate may not be essential for toxicity. Additionally, IAPP_{A25P}
34
35 showed a tendency to occupy lower oligomeric states than other variants. The studies which lead
36
37 to the model directly probed the FGAIL region, but positions 28 and 29⁶⁵. The results with the
38
39 S28P substitution suggest that S28 is part of the transient β -sheet or that residues outside of the
40
41 putative β -sheet intermediate play a significant role in modulating amyloidogenicity. The results
42
43 with the S29P variant argues that this site is outside of the critical region of the β -sheet
44
45 intermediate.
46
47
48
49
50
51
52
53
54
55
56
57
58
59
60

1
2
3 The IM-MS studies reveal that there is no detectable correlation between gas phase
4 structure as judged by the CSS and the kinetics of IAPP amyloid formation. The structural
5 features which lead to the significant variation in lag times are either not manifested in the
6 conformations of the monomer and dimers or are too subtle to be detected via the CCS
7 measurements.
8
9

10
11
12 Overall, while the general trends of proline substitutions on the time to form amyloid
13 were predicted by the amyloid prediction algorithms examined in this study the methods did not
14 reproduced the exact order. The A25P substitution was predicted to have the largest effect on
15 amyloid formation by four out of five methods, in contrast to the experimental results, however
16 both A25P and S28P were predicted to have the largest impact on amyloid formation.
17
18 Additionally, double proline substitutions were scored less amyloidogenic than single proline
19 substitutions. Thus, the existing algorithms do not capture all of the details.
20
21
22
23
24
25
26
27
28
29

30
31 It is also interesting to compare the experimental results to the results of molecular
32 dynamics simulations⁶⁷⁻⁶⁹. Recent work has shown that standard force fields with standard water
33 models often lead to overly compact ensembles for IDP's and unfolded protein states, although
34 this issue is being addressed⁷⁰⁻⁷⁴. Individual MD methods can also have unique biases for local
35 structure, thus we believe caution is warranted when interpreting the results of MD simulations
36 of IAPP. Molecular dynamics studies of IAPP fragments have previously suggested A25P to be
37 responsible for rIAPP's non-amyloidogenic properties by means of its disruption of a β -turn,
38 while other molecular dynamics studies have suggested that the S28P substitution promotes a
39 local helical conformation^{67, 68}. This stabilized helix structure was hypothesized to prolong
40 aggregation by preventing the formation of local β -sheet structure. Additionally, it has been
41 proposed that the S28P mutation effects compaction of the IAPP monomer, although we do not
42
43
44
45
46
47
48
49
50
51
52
53
54
55
56
57
58
59
60

1
2
3 detect this in our IMS-MS studies⁶⁹. The experimental work presented here shows that MD
4
5 simulations are not yet at a point where they can precisely capture features that accurately predict
6
7 IAPP amyloidogenicity. We hope that the data presented here will aid efforts to validate
8
9 simulations of IAPP.
10

11
12 Cell viability assays results showed that IAPP_{S28P}, as well as double analogs containing a
13
14 S28P substitution exhibit a significant reduction in cytotoxicity in contrast, variants which lack
15
16 the S28P substitution exhibit a smaller reduction in cytotoxic. Particularly interesting is the
17
18 comparison of the S28P and S29P substitutions. These identical replacements located
19
20 immediately adjacent to each other have vastly different effects on toxicity. Doubly substituted
21
22 variants containing the S28P replacement were the least cytotoxic, showing minimal changes in
23
24 metabolic health and minimal membrane disruption at concentrations up to at least 250 μM ; the
25
26 EC_{50} value of the S28P, S29P double analog is clearly greater than 300 μM . The demonstration
27
28
29
30 that the S28P replacement has the largest impact on reducing cytotoxicity will prove useful in the
31
32 design of next generation soluble hIAPP variants. Comparisons of the two cytotoxicity assays
33
34 provides addition insight into IAPP mediated cytotoxicity. The data indicates that the cell
35
36 membrane is permeabilized at lower concentrations than needed to significantly disrupt overall
37
38 cell health (as judged by global ATP levels). The studies reported here involve studies as a
39
40 function of peptide concentration, but do not provide time resolved information, thus we
41
42 formally cannot determine if membrane permeabilization is up stream of the disruption of overall
43
44 cell health.
45
46
47
48
49
50

51
52 The observation that the A25P substitution and the IAPP_{A25P S29P} double analogs have
53
54 only a modest effect upon toxicity, but significantly prolong the lag phase, while still forming
55
56
57

1
2
3 amyloid indicates that they could be very useful model systems for interrogating the
4
5 conformational propensities of toxic IAPP oligomers. The longer lag phase should help facilitate
6
7 structural studies. For example, comparative structural studies of the S28P and S29P single
8
9 analogs and comparative studies of the S28P S29P double and A25P, S29P double analogs may
10
11 provide more insight into the features which link sequence to amyloidogenicity and toxicity and
12
13 are the subject of future work. Such studies are outside the scope of the current work.
14
15
16

17
18 Overall the work reveals the plasticity of IAPP amyloid formation in that the polypeptide
19
20 can still form amyloid even when two residues in the interface between the two stacks of
21
22 monomers are replaced with proline. From another perspective, the comparative studies of the
23
24 effects of S28P and S29P replacements in the double and single analogs reveal the pronounced
25
26 sequence sensitivity of IAPP toxicity and amyloidogenicity and provide insight into the rational
27
28 design of non-amyloidogenic non-toxic variants of human IAPP.
29
30
31

32 **Associated Content**

33
34 **Supporting Information** Supporting Information is available free of charge on the ACS
35
36 publications website at DOI:

37
38
39 A table of predicted amyloidogenic regions of hIAPP and variants as calculated by the WALTZ
40
41 algorithm. A table of the calculated aggregation propensities of hIAPP and variants as calculated
42
43 by the TANGO algorithm. A table of the calculated aggregation propensities of hIAPP and
44
45 variants as calculated by the PASTA algorithm. A table of the calculated aggregation
46
47 propensities of hIAPP and variants as calculated by the AGGRESCAN algorithm. A figure
48
49 predicted amyloid forming regions of hIAPP and variants as calculated by the ZipperDB
50
51 algorithm. A figure of thioflavin-T kinetics and TEM of S28P containing variants at 100 μ M
52
53 peptide concentration. A Figure of thioflavin-T curves collected in triplicate for all variants,
54
55
56
57

1
2
3 curve slopes, and maximum fluorescence intensities. Figures of the CSS calibration curves used
4 during each day of IM-MS data collection. A figure of unsmoothed arrival time distributions for
5 hIAPP and variants. Comparison of relative populations of dimeric and monomeric for hIAPP
6 variants compared to T_{50} and EC_{50} . A figure showing the results of PICUP studies on hIAPP and
7 variants.
8
9

14 **Accession Codes**

15 IAPP, UniProtKB P10997
16
17
18
19
20

21 **Acknowledgements.** Support from US National Institutes of Health grant GM078114 and
22 Wellcome Trust award 107927/Z/15/Z and a BBSRC iCASE PhD studentship (CH) with Waters
23 BB/L015382/1. ZR was supported in part by a GAANN fellowship from the US Department of
24 Education. The IM-MS spectrometry was purchased via Wellcome Trust Multiuser equipment
25 grant 104913/Z/14/Z to KT.
26
27
28
29
30
31
32
33
34
35
36
37
38
39
40
41
42
43
44
45
46
47
48
49
50
51
52
53
54
55
56
57
58
59
60

References

- [1] Eisenberg, D., and Jucker, M. (2012) The amyloid state of proteins in human diseases, *Cell* 148, 1188-1203.
- [2] Chiti, F., and Dobson, C. M. (2017) Protein Misfolding, Amyloid Formation, and Human Disease: A Summary of Progress Over the Last Decade, *Annual Review of Biochemistry* 86, 27-68.
- [3] Riek, R., and Eisenberg, D. S. (2016) The activities of amyloids from a structural perspective, *Nature* 539, 227-235.
- [4] Westermark, P., Andersson, A., and Westermark, G. T. (2011) Islet Amyloid Polypeptide, Islet Amyloid, and Diabetes Mellitus, *Physiology Reviews* 91, 795-826.
- [5] Akter, R., Cao, P., Noor, H., Ridgway, Z., Tu, L.-H., Wang, H., Wong, A. G., Zhang, X., Abedini, A., Schmidt, A. M., and Raleigh, D. P. (2016) Islet Amyloid Polypeptide: Structure, Function, and Pathophysiology, *Journal of Diabetes Research* 2016, ID 2798269.
- [6] Cooper, G. J., Leighton, B., Dimitriadis, G. D., Parry-Billings, M., Kowalchuk, J. M., Howland, K., Rothbard, J. B., Willis, A. C., and Reid, K. B. (1988) Amylin found in amyloid deposits in human type 2 diabetes mellitus may be a hormone that regulates glycogen metabolism in skeletal muscle, *Proceedings of the National Academy of Sciences of the United States of America* 85, 7763-7766.
- [7] Westermark, P., Wernstedt, C., Wilander, E., Hayden, D. W., O'Brien, T. D., and Johnson, K. H. (1987) Amyloid fibrils in human insulinoma and islets of Langerhans of the diabetic cat are derived from a neuropeptide-like protein also present in normal islet cells, *Proceedings of the National Academy of Sciences of the United States of America* 84, 3881-3885.
- [8] Potter, K. J., Abedini, A., Marek, P., Klimek, A. M., Butterworth, S., Driscoll, M., Baker, R., Nilsson, M. R., Warnock, G. L., Oberholzer, J., Bertera, S., Trucco, M., Korbutt, G. S., Fraser, P. E., Raleigh, D. P., and Verchere, C. B. (2010) Islet amyloid deposition limits the viability of human islet grafts but not porcine islet grafts, *Proceedings of the National Academy of Sciences of the United States of America* 107, 4305-4310.
- [9] Udayasankar, J., Kodama, K., Hull, R. L., Zraika, S., Aston-Mourney, K., Subramanian, S. L., Tong, J., Faulenbach, M. V., Vidal, J., and Kahn, S. E. (2009) Amyloid formation results in recurrence of hyperglycaemia following transplantation of human IAPP transgenic mouse islets, *Diabetologia* 52, 145-153.
- [10] Abedini, A., and Schmidt, A. M. (2013) Mechanisms of Islet Amyloidosis Toxicity in Type 2 Diabetes, *FEBS Letters* 587, 1119-1127.
- [11] Raleigh, D., Zhang, X., Hastoy, B., and Clark, A. (2017) The beta-cell assassin: IAPP cytotoxicity, *Journal of Molecular Endocrinology* 59, R121-r140.
- [12] Abedini, A., Plesner, A., Cao, P., Ridgway, Z., Zhang, J., Tu, L.-H., Middleton, C. T., Chao, B., Sartori, D. J., Meng, F., Wang, H., Wong, A. G., Zanni, M. T., Verchere, C. B., Raleigh, D. P., and Schmidt, A. M. (2016) Time-resolved studies define the nature of toxic IAPP intermediates, providing insight for anti-amyloidosis therapeutics, *eLife* 5, e12977.
- [13] Costes, S. (2018) Targeting protein misfolding to protect pancreatic beta-cells in type 2 diabetes, *Current Opinion in Pharmacology* 43, 104-110.
- [14] Kahn, S. E., Zraika, S., Utzschneider, K. M., and Hull, R. L. (2009) The beta cell lesion in type 2 diabetes: there has to be a primary functional abnormality, *Diabetologia* 52, 1003-1012.
- [15] Denroche, H. C., and Verchere, C. B. (2018) IAPP and type 1 diabetes: implications for immunity, metabolism and islet transplants, *Journal of Molecular Endocrinology* 60, R57-r75.
- [16] Westermark, G. T., Krogvold, L., Dahl-Jørgensen, K., and Ludvigsson, J. (2017) Islet amyloid in recent-onset type 1 diabetes-the DiViD study, *Upsala Journal of Medical Science* 122, 201-203.
- [17] Kahn, S. E., Templin, A. T., Hull, R. L., and Verchere, C. B. (2019) Probing the Meaning of Persistent Propeptide Release in Type 1 Diabetes, *Diabetes Care* 42, 183-185.

- 1
2
3 [18] Wu, C., and Shea, J.-E. (2013) Structural Similarities and Differences between Amyloidogenic and
4 Non-Amyloidogenic Islet Amyloid Polypeptide (IAPP) Sequences and Implications for the Dual
5 Physiological and Pathological Activities of These Peptides, *PLOS Computational Biology* 9,
6 e1003211.
- 7 [19] Akter, R., Abedini, A., Ridgway, Z., Zhang, X., Kleinberg, J., Schmidt, A. M., and Raleigh, D. P.
8 (2017) Evolutionary Adaptation and Amyloid Formation: Does the Reduced Amyloidogenicity
9 and Cytotoxicity of Ursine Amylin Contribute to the Metabolic Adaption of Bears and Polar
10 Bears?, *Israel Journal of Chemistry* 57, 750-761.
- 11 [20] Akter, R., Bower, R. L., Abedini, A., Schmidt, A. M., Hay, D. L., and Raleigh, D. P. (2018)
12 Amyloidogenicity, Cytotoxicity, and Receptor Activity of Bovine Amylin: Implications for
13 Xenobiotic Transplantation and the Design of Nontoxic Amylin Variants, *ACS Chemical Biology*
14 13, 2747-2757.
- 15 [21] Betsholtz, C., Christmansson, L., Engström, U., Rorsman, F., Svensson, V., Johnson, K. H., and
16 Westermark, P. (1989) Sequence divergence in a specific region of islet amyloid polypeptide
17 (IAPP) explains differences in islet amyloid formation between species, *FEBS Letters* 251, 261-
18 264.
- 19 [22] Cao, P., Meng, F., Abedini, A., and Raleigh, D. P. (2010) The Ability of Rodent Islet Amyloid
20 Polypeptide To Inhibit Amyloid Formation by Human Islet Amyloid Polypeptide Has Important
21 Implications for the Mechanism of Amyloid Formation and the Design of Inhibitors,
22 *Biochemistry* 49, 872-881.
- 23 [23] Westermark, P., Engström, U., Johnson, K. H., Westermark, G. T., and Betsholtz, C. (1990) Islet
24 amyloid polypeptide: pinpointing amino acid residues linked to amyloid fibril formation,
25 *Proceedings of the National Academy of Sciences of the United States of America* 87, 5036-5040.
- 26 [24] Ryan, G., Briscoe, T. A., and Jobe, L. (2009) Review of pramlintide as adjunctive therapy in
27 treatment of type 1 and type 2 diabetes, *Drug design, Development and Therapy* 2, 203-214.
- 28 [25] Isaacs, D., Yager, S., Parker, M., Wolfe, L., Luxenburg, J., and Lekic, S. (2019) Adjunct
29 Antihyperglycemic Agents in Overweight and Obese Adults With Type 1 Diabetes, *The Annals of*
30 *Pharmacotherapy* 53, 371-384.
- 31 [26] da Silva, D. C., Fontes, G. N., Erthal, L. C. S., and Lima, L. M. T. R. (2016) Amyloidogenesis of the
32 amylin analogue pramlintide, *Biophysical Chemistry* 219, 1-8.
- 33 [27] Wiltzius, J. J. W., Sievers, S. A., Sawaya, M. R., Cascio, D., Popov, D., Riek, C., and Eisenberg,
34 D. (2008) Atomic Structure of The Cross-Beta Spine of Islet Amyloid Polypeptide (Amylin),
35 *Protein Science* 17, 1467-1474.
- 36 [28] Luca, S., Yau, W. M., Leapman, R., and Tycko, R. (2007) Peptide Conformation and
37 Supramolecular Organization in Amylin Fibrils: Constraints From Solid-State NMR,
38 *Biochemistry* 46, 13505-13522.
- 39 [29] Nguyen, P. T., Zottig, X., Sebastiao, M., and Bourgault, S. (2017) Role of Site-Specific Asparagine
40 Deamidation in Islet Amyloid Polypeptide Amyloidogenesis: Key Contributions of Residues 14
41 and 21, *Biochemistry* 56, 3808-3817.
- 42 [30] Koo, B. W., Hebda, J. A., and Miranker, A. D. (2008) Amide inequivalence in the fibrillar assembly
43 of islet amyloid polypeptide, *Protein Engineering, Design & Selection : PEDS* 21, 147-154.
- 44 [31] Marek, P., Woys, A. M., Sutton, K., Zanni, M. T., and Raleigh, D. P. (2010) Efficient Microwave
45 Assisted Synthesis of Human Islet Amyloid Polypeptide Designed to Facilitate The Specific
46 Incorporation of Labeled Amino Acids, *Organic Letters* 12, 4848-4851.
- 47 [32] Abedini, A., and Raleigh, D. P. (2005) Incorporation of Pseudoproline Derivatives Allows the Facile
48 Synthesis of Human IAPP, a Highly Amyloidogenic and Aggregation-Prone Polypeptide,
49 *Organic Letters* 7, 693-696.
- 50 [33] Nilsson, M. R., and Raleigh, D. P. (1999) Analysis of amylin cleavage products provides new
51 insights into the amyloidogenic region of human amylin, *Journal of Molecular Biology* 294,
52 1375-1385.
- 53
54
55
56
57
58
59
60

- 1
2
3 [34] Xue, C., Lin, T. Y., Chang, D., and Guo, Z. (2017) Thioflavin T as an amyloid dye: fibril
4 quantification, optimal concentration and effect on aggregation, *Royal Society Open Science* 4,
5 160696-160696.
- 6 [35] Tu, L.-H., and Raleigh, D. P. (2013) Role of Aromatic Interactions in Amyloid Formation by Islet
7 Amyloid Polypeptide, *Biochemistry* 52, 333-342.
- 8 [36] Sebastiao, M., Quittot, N., and Bourgault, S. (2017) Thioflavin T fluorescence to analyse amyloid
9 formation kinetics: Measurement frequency as a factor explaining irreproducibility, *Analytical*
10 *Biochemistry* 532, 83-86.
- 11 [37] Haler, J. R. N., Massonnet, P., Chirot, F., Kune, C., Comby-Zerbino, C., Jordens, J., Honing, M.,
12 Mengerink, Y., Far, J., Dugourd, P., and De Pauw, E. (2018) Comparison of Different Ion
13 Mobility Setups Using Poly (Ethylene Oxide) PEO Polymers: Drift Tube, TIMS, and T-Wave,
14 *Journal of The American Society for Mass Spectrometry* 29, 114-120.
- 15 [38] Haler, J. R. N., Kune, C., Massonnet, P., Comby-Zerbino, C., Jordens, J., Honing, M., Mengerink,
16 Y., Far, J., and De Pauw, E. (2017) Comprehensive Ion Mobility Calibration: Poly(ethylene
17 oxide) Polymer Calibrants and General Strategies, *Analytical Chemistry* 89, 12076-12086.
- 18 [39] Valentine, S. J., Counterman, A. E., and Clemmer, D. E. (1999) A database of 660 peptide ion cross
19 sections: Use of intrinsic size parameters for bona fide predictions of cross sections, *Journal of*
20 *the American Society for Mass Spectrometry* 10, 1188-1211.
- 21 [40] Thalassinos, K., Grabenauer, M., Slade, S. E., Hilton, G. R., Bowers, M. T., and Scrivens, J. H.
22 (2009) Characterization of Phosphorylated Peptides Using Traveling Wave-Based and Drift Cell
23 Ion Mobility Mass Spectrometry, *Analytical Chemistry* 81, 248-254.
- 24 [41] Gabelica, V., Shvartsburg, A. A., Afonso, C., Barran, P., Benesch, J. L. P., Bleiholder, C., Bowers,
25 M. T., Bilbao, A., Bush, M. F., Campbell, J. L., Campuzano, I. D. G., Causon, T., Clowers, B. H.,
26 Creaser, C. S., De Pauw, E., Far, J., Fernandez-Lima, F., Fjeldsted, J. C., Giles, K., Groessl, M.,
27 Hogan Jr, C. J., Hann, S., Kim, H. I., Kurulugama, R. T., May, J. C., McLean, J. A., Pagel, K.,
28 Richardson, K., Ridgeway, M. E., Rosu, F., Sobott, F., Thalassinos, K., Valentine, S. J., and
29 Wyttenbach, T. (2019) Recommendations for reporting ion mobility Mass Spectrometry
30 measurements, *Mass Spectrometry Reviews* 38, 291-320.
- 31 [42] Nelson, R., Sawaya, M. R., Balbirnie, M., Madsen, A. Ø., Riek, C., Grothe, R., and Eisenberg, D.
32 (2005) Structure of the cross-beta spine of amyloid-like fibrils, *Nature* 435, 773-778.
- 33 [43] Tsai, H.-H. G., Reches, M., Tsai, C.-J., Gunasekaran, K., Gazit, E., and Nussinov, R. (2005) Energy
34 landscape of amyloidogenic peptide oligomerization by parallel-tempering molecular dynamics
35 simulation: significant role of Asn ladder, *Proceedings of the National Academy of Sciences of*
36 *the United States of America* 102, 8174-8179.
- 37 [44] Wong, A. G., Wu, C., Hannaberry, E., Watson, M. D., Shea, J.-E., and Raleigh, D. P. (2016)
38 Analysis of the Amyloidogenic Potential of Pufferfish (*Takifugu rubripes*) Islet Amyloid
39 Polypeptide Highlights the Limitations of Thioflavin-T Assays and the Difficulties in Defining
40 Amyloidogenicity, *Biochemistry* 55, 510-518.
- 41 [45] LeVine, H. (1999) [18] Quantification of β -sheet amyloid fibril structures with thioflavin T, In
42 *Methods in Enzymology*, pp 274-284, Academic Press.
- 43 [46] Goldschmidt, L., Teng, P. K., Riek, R., and Eisenberg, D. (2010) Identifying the amyloids, proteins
44 capable of forming amyloid-like fibrils, *Proceedings of the National Academy of Sciences of the*
45 *United States of America* 107, 3487-3492.
- 46 [47] Maurer-Stroh, S., Debulpaep, M., Kuemmerer, N., de la Paz, M. L., Martins, I. C., Reumers, J.,
47 Morris, K. L., Copland, A., Serpell, L., Serrano, L., Schymkowitz, J. W. H., and Rousseau, F.
48 (2010) Exploring the sequence determinants of amyloid structure using position-specific scoring
49 matrices, *Nature Methods* 7, 237-242.
- 50 [48] Fernandez-Escamilla, A.-M., Rousseau, F., Schymkowitz, J., and Serrano, L. (2004) Prediction of
51 Sequence-Dependent And Mutational Effects on the Aggregation of Peptides and Proteins,
52 *Nature Biotechnology* 22, 1302-1306.
- 53
54
55
56
57
58
59
60

- 1
2
3 [49] Trovato, A., Seno, F., and Tosatto, S. C. E. (2007) The PASTA server for protein aggregation
4 prediction, *Protein Engineering, Design and Selection* 20, 521-523.
- 5 [50] Conchillo-Solé, O., de Groot, N. S., Avilés, F. X., Vendrell, J., Daura, X., and Ventura, S. (2007)
6 AGGRESCAN: a server for the prediction and evaluation of "hot spots" of aggregation in
7 polypeptides, *BMC Bioinformatics* 8, 65.
- 8 [51] Viehland, L. A., and Mason, E. A. (1978) Gaseous ion mobility and diffusion in electric fields of
9 arbitrary strength, *Annals of Physics* 110, 287-328.
- 10 [52] Dupuis, N. F., Wu, C., Shea, J.-E., and Bowers, M. T. (2009) Human Islet Amyloid Polypeptide
11 Monomers Form Ordered β -hairpins: A Possible Direct Amyloidogenic Precursor, *Journal of the*
12 *American Chemical Society* 131, 18283-18292.
- 13 [53] Dupuis, N. F., Wu, C., Shea, J.-E., and Bowers, M. T. (2011) The Amyloid Formation Mechanism in
14 Human IAPP: Dimers Have β -Strand Monomer–Monomer Interfaces, *Journal of the American*
15 *Chemical Society* 133, 7240-7243.
- 16 [54] Young, L. M., Tu, L.-H., Raleigh, D. P., Ashcroft, A. E., and Radford, S. E. (2017) Understanding
17 co-polymerization in amyloid formation by direct observation of mixed oligomers, *Chemical*
18 *Science* 8, 5030-5040.
- 19 [55] Young, L. M., Cao, P., Raleigh, D. P., Ashcroft, A. E., and Radford, S. E. (2014) Ion Mobility
20 Spectrometry–Mass Spectrometry Defines the Oligomeric Intermediates in Amylin Amyloid
21 Formation and the Mode of Action of Inhibitors, *Journal of the American Chemical Society* 136,
22 660-670.
- 23 [56] Tu, L. H., Young, L. M., Wong, A. G., Ashcroft, A. E., Radford, S. E., and Raleigh, D. P. (2015)
24 Mutational analysis of the ability of resveratrol to inhibit amyloid formation by islet amyloid
25 polypeptide: critical evaluation of the importance of aromatic-inhibitor and histidine-inhibitor
26 interactions, *Biochemistry* 54, 666-676.
- 27 [57] Young, L. M., Mahood, R. A., Saunders, J. C., Tu, L. H., Raleigh, D. P., Radford, S. E., and
28 Ashcroft, A. E. (2015) Insights into the consequences of co-polymerisation in the early stages of
29 IAPP and A β peptide assembly from mass spectrometry, *The Analyst* 140, 6990-6999.
- 30 [58] Riba, I., Barran, P. E., Cooper, G. J. S., and Unwin, R. D. (2015) On the structure of the copper–
31 amylin complex, *International Journal of Mass Spectrometry* 391, 47-53.
- 32 [59] Li, H., Ha, E., Donaldson, R. P., Jeremic, A. M., and Vertes, A. (2015) Rapid Assessment of Human
33 Amylin Aggregation and Its Inhibition by Copper(II) Ions by Laser Ablation Electrospray
34 Ionization Mass Spectrometry with Ion Mobility Separation, *Analytical Chemistry* 87, 9829-9837.
- 35 [60] Saunders, J. C., Young, L. M., Mahood, R. A., Jackson, M. P., Revill, C. H., Foster, R. J., Smith, D.
36 A., Ashcroft, A. E., Brockwell, D. J., and Radford, S. E. (2016) An in vivo platform for
37 identifying inhibitors of protein aggregation, *Nature Chemical Biology* 12, 94-101.
- 38 [61] Young, L. M., Saunders, J. C., Mahood, R. A., Revill, C. H., Foster, R. J., Ashcroft, A. E., and
39 Radford, S. E. (2016) ESI-IMS–MS: A method for rapid analysis of protein aggregation and its
40 inhibition by small molecules, *Methods* 95, 62-69.
- 41 [62] Sivalingam, G. N., Cryar, A., Williams, M. A., Gooptu, B., and Thalassinos, K. (2018)
42 Deconvolution of ion mobility mass spectrometry arrival time distributions using a genetic
43 algorithm approach: Application to α 1-antitrypsin peptide binding, *International Journal of Mass*
44 *Spectrometry* 426, 29-37.
- 45 [63] Eldrid, C., Ujma, J., Kalfas, S., Tomczyk, N., Giles, K., Morris, M., and Thalassinos, K. (2019) Gas
46 Phase Stability of Protein Ions in a Cyclic Ion Mobility Spectrometry Traveling Wave Device,
47 *Analytical Chemistry* 91, 7554-7561.
- 48 [64] Bitan, G., and Teplow, D. B. (2004) Rapid Photochemical Cross-Linking A New Tool for Studies of
49 Metastable, Amyloidogenic Protein Assemblies, *Accounts of Chemical Research* 37, 357-364.
- 50 [65] Buchanan, L. E., Dunkelberger, E. B., Tran, H. Q., Cheng, P.-N., Chiu, C.-C., Cao, P., Raleigh, D.
51 P., de Pablo, J. J., Nowick, J. S., and Zanni, M. T. (2013) Mechanism of IAPP amyloid fibril
52 formation involves an intermediate with a transient β -sheet, *Proceedings of the National Academy*
53 *of Sciences of the United States of America* 110, 19285-19290.
- 54
55
56
57
58
59
60

- 1
2
3 [66] Serrano, A. L., Lomont, J. P., Tu, L. H., Raleigh, D. P., and Zanni, M. T. (2017) A Free Energy
4 Barrier Caused by the Refolding of an Oligomeric Intermediate Controls the Lag Time of
5 Amyloid Formation by hIAPP, *Journal of the American Chemical Society* 139, 16748-16758.
- 6 [67] Andrews, M. N., and Winter, R. (2011) Comparing the structural properties of human and rat islet
7 amyloid polypeptide by MD computer simulations, *Biophysical Chemistry* 156, 43-50.
- 8 [68] Chakraborty, S., Chatterjee, B., and Basu, S. (2012) A Mechanistic Insight into the Amyloidogenic
9 Structure of hIAPP Peptide Revealed From Sequence Analysis and Molecular Dynamics
10 Simulation, *Biophysical Chemistry* 168, 1-9.
- 11 [69] Andrews, M. (2014) *Molecular Dynamics of Monomeric IAPP in Solution: A Study of IAPP in Water*
12 *at the Percolation Transition*, Anchor Academic Publishing.
- 13 [70] Wang, L.-P., McKiernan, K. A., Gomes, J., Beauchamp, K. A., Head-Gordon, T., Rice, J. E., Swope,
14 W. C., Martínez, T. J., and Pande, V. S. (2017) Building a More Predictive Protein Force Field: A
15 Systematic and Reproducible Route to AMBER-FB15, *The Journal of Physical Chemistry B* 121,
16 4023-4039.
- 17 [71] Huang, J., Rauscher, S., Nawrocki, G., Ran, T., Feig, M., de Groot, B. L., Grubmüller, H., and
18 MacKerell Jr, A. D. (2016) CHARMM36m: an improved force field for folded and intrinsically
19 disordered proteins, *Nature Methods* 14, 71-73.
- 20 [72] Robustelli, P., Piana, S., and Shaw, D. E. (2018) Developing a molecular dynamics force field for
21 both folded and disordered protein states, *Proceedings of the National Academy of Sciences of the*
22 *United States of America* 115, E4758-E4766
- 23 [73] Rauscher, S., Gapsys, V., Gajda, M. J., Zweckstetter, M., de Groot, B. L., and Grubmüller, H. (2015)
24 Structural Ensembles of Intrinsically Disordered Proteins Depend Strongly on Force Field: A
25 Comparison to Experiment, *Journal of Chemical Theory and Computation* 11, 5513-5524.
- 26 [74] Best, R. B. (2017) Computational and theoretical advances in studies of intrinsically disordered
27 proteins, *Current Opinion in Structural Biology* 42, 147-154.
28
29
30
31
32
33
34
35
36
37
38
39
40
41
42
43
44
45
46
47
48
49
50
51
52
53
54
55
56
57
58
59
60

1
2
3
4
5
6 For Table of Contents use Only
7
8
9

